9-1-2018

Adipose Tissue Dysfunction Occurs Independently of Obesity in Adipocyte-Specific Oncostatin Receptor Knockout Mice

Jacqueline M. Stephens
Pennington Biomedical Research Center

Jennifer L. Bailey
Pennington Biomedical Research Center

Hardy Hang
Pennington Biomedical Research Center

Victoria Rittell
Pennington Biomedical Research Center

Marilyn A. Dietrich
Pennington Biomedical Research Center

See next page for additional authors

Recommended Citation

Stephens, J., Bailey, J., Hang, H., Rittell, V., Dietrich, M., Mynatt, R., & Elks, C. (2018). Adipose Tissue Dysfunction Occurs Independently of Obesity in Adipocyte-Specific Oncostatin Receptor Knockout Mice. *Obesity, 26* (9), 1439-1447. https://doi.org/10.1002/oby.22254

Published in final edited form as:

Obesity (Silver Spring). 2018 September ; 26(9): 1439–1447. doi:10.1002/oby.22254.

Adipose Tissue Dysfunction Occurs Independently of Obesity in Adipocyte-Specific Oncostatin Receptor Knockout Mice

Jacqueline M. Stephens[1], **Jennifer L. Bailey**[2], **Hardy Hang**[1], **Victoria Rittell**[1,2], **Marilyn A. Dietrich**[3], **Randall L. Mynatt**[4], and **Carrie M. Elks**[2,*]

[1]Adipocyte Biology Laboratory, Pennington Biomedical Research Center, Baton Rouge, LA, 70808

[2]Matrix Biology Laboratory, Pennington Biomedical Research Center, Baton Rouge, LA, 70808

[3]Cell Biology and Bioimaging Core, Pennington Biomedical Research Center, Baton Rouge, LA, 70808

[4]Transgenics Core, Pennington Biomedical Research Center, Baton Rouge, LA, 70808

Abstract

Objective—This study examined the phenotypic effects of adipocyte-specific oncostatin M receptor (OSMR) loss in chow-fed mice.

Methods—Chow-fed adipocyte-specific OSMR knockout (FKO) mice and littermate $OSMR^{fl/fl}$ controls were studied. Tissue weights, insulin sensitivity, adipokine production, and stromal cell immunophenotypes were assessed in epididymal fat (eWAT); serum adipokine production was also assessed. *In vitro*, adipocytes were treated with oncostatin M (OSM) and adipokine gene expression assessed.

Results—Body weights, fasting blood glucose levels, and eWAT weights did not differ between genotypes. However, the eWAT of $OSMR^{FKO}$ mice was modestly less responsive to insulin stimulation than that of $OSMR^{fl/fl}$ mice. Notably, significant increases in adipokines including C-reactive protein, lipocalin 2, intercellular adhesion molecule-1 (ICAM-1), and insulin-like growth factor binding protein 6, were observed in the eWAT of $OSMR^{FKO}$ mice. In addition, significant increases in fetuin A and ICAM-1 were detected in $OSMR^{FKO}$ serum. Flow cytometry revealed a significant increase in leukocyte number and modest, but not statistically significant, increases in B and T cells in the eWAT of $OSMR^{FKO}$ mice.

Conclusions—The chow-fed $OSMR^{FKO}$ mouse exhibits adipose tissue dysfunction and increased pro-inflammatory adipokine production. These results suggest that intact adipocyte OSM-OSMR signaling is necessary for adipose tissue immune cell homeostasis.

*Corresponding Author: Carrie M. Elks, PhD, RD, Matrix Biology Laboratory, Pennington Biomedical Research Center, 6400 Perkins Road, Baton Rouge, LA 70808, USA, Phone: (225) 763-3140, carrie.elks@pbrc.edu.

Disclosure: The authors declare no conflict of interest

Keywords

adipose tissue; inflammation; oncostatin M; adipokines

INTRODUCTION

A coordination among healthy adipocytes and stromal vascular cells (SVCs, including immune cells, preadipocytes, and endothelial cells) in the local adipose tissue environment is critical to maintain homeostasis of both adipose tissue and systemic metabolism. Obesity is intimately coupled to a chronic, low-grade inflammatory state characterized by leukocyte infiltration of adipose tissue and subsequent modulation of the tissue adipokine profile. Activation of infiltrating leukocytes and promotion of pro-inflammatory adipokine production can enable adipose tissue dysfunction and lead to temporal effects on metabolic homeostasis (1, 2, 3, 4).

Oncostatin M (OSM), an adipokine belonging to the interleukin-6/gp130 family of cytokines, regulates a variety of physiological and pathological processes (5, 6). First recognized in 1986 for its anti-tumorigenic effects (7), it is now evident that OSM can regulate many other biological processes in a cell-type dependent manner (8). OSM is a unique gp130 cytokine in that it has its own specific receptor subunit (OSM receptor β or OSMR) that heterodimerizes with gp130 to create a functional OSM receptor complex, which produces the majority of OSM effects (9). Adipocytes in particular exhibit extensive responses to OSM (10, 11), and OSMR is highly expressed in adipose tissue (12). Importantly, though adipocytes express OSMR, they do not produce OSM itself. Rather, OSM is produced in various adipose tissue SVCs including macrophages, T cells, and B cells (10, 12). Increased adipose tissue expression of OSM and OSMR are correlates of obesity in both mouse and man (12). We have previously shown that adipocyte-specific deletion of OSMR in mice (referred to here as $OSMR^{FKO}$ mice) is associated with augmented adipose tissue inflammation and systemic insulin resistance and obesity (10). Notably, adipose tissue OSM expression itself is elevated in obese $OSMR^{FKO}$ mice (10). While we have demonstrated its role in perpetuating inflammation and systemic insulin resistance in the obese condition (10), it remains unclear what potential effects disrupted adipose tissue OSM signaling has in the absence of obesity.

With the present study, we examined the function of adipose tissue OSM signaling in the absence of an obesogenic stimulus such as a high-fat diet. Our novel observations demonstrate that, in the absence of obesity, $OSMR^{FKO}$ mice exhibit leukocyte accumulation, increased pro-inflammatory adipokine production, and a modest reduction of adipose tissue insulin responsiveness. These effects occur in the absence of differences in body weight or adiposity. These results corroborate our previous observations that intact adipocyte OSM signaling is necessary for maintenance of adipose tissue homeostasis, and demonstrate that adipose tissue dysfunction precedes systemic metabolic dysfunction in this model.

METHODS

Animals and Husbandry

Mixed background OSMR^{FKO} mice and homozygous floxed littermates (OSMR$^{fl/fl}$) were obtained from our in-house colony, which was generated using adiponectin–Cre and OSMR floxed mice as previously described (10). All mice used in these studies were male, were 6–9 months of age, and were maintained on LabDiet #5015 (LabDiet, St. Louis, MO) from weaning (3 weeks of age) until study termination. Mice were housed in a temperature (22° ± 2° Celsius) - and humidity-controlled (45–55%) room under a 12-hour light/dark cycle, and allowed *ad libitum* access to food and water. Tissue OSMR and gp130 gene and protein expression, 4-hour blood glucose measurement, and eWAT insulin sensitivity studies (acute intraperitoneal insulin injections) were performed on one cohort of mice. Acute OSM injection studies were conducted in a second cohort of mice, tissue adipokine studies were conducted in mice from the protein expression cohort and in a third cohort. Serum adipokine studies were also conducted in third cohort. Flow cytometry studies were performed in an additional cohort of 6-month old mice. The Pennington Biomedical Research Center Institutional Animal Care and Use Committee approved all studies (protocol #961P).

Acute OSM injection experiments

Fed mice (n=4 OSMR$^{fl/fl}$ and n=4 OSMR^{FKO}) were given acute injections of 200 ng recombinant murine OSM (mOSM; R&D Systems; Minneapolis, MN; catalog #495-MO-025) or vehicle (sterile 0.1% BSA in PBS) and sacrificed 15 minutes later. Epididymal fat pads were excised, snap frozen, and stored at −80°C for immunoblotting analyses as described below.

Cell culture and treatments

Murine 3T3-L1 preadipocytes were grown to 2 days post-confluence in DMEM with 10% fetal bovine serum (FBS) and differentiated as described previously (10). One day prior to beginning OSM treatment of adipocytes, medium was replaced with DMEM containing 5% FBS. Cells were pretreated with 50 μM of the ERK inhibitor U0126 for 1 hour, and then 1nM recombinant mOSM or vehicle (0.1% BSA in PBS) was added as indicated. Six hours later, medium was removed, and cells were washed with PBS and then harvested for RNA extraction. Experiments were performed in duplicate.

Gene expression analyses

Total RNA was isolated from indicated mouse tissues or 3T3-L1 adipocytes using an RNeasy Mini Kit (Qiagen; Germantown, MD) and yield determined by spectrophotometry (NanoDrop Technologies; Wilmington, DE) as previously described (10). cDNA was synthesized using the High Capacity cDNA Reverse Transcription kit (Applied Biosystems; Foster City, CA) with the SYBR Green system (Clontech; Mountain View, CA). Relative quantification of mRNA expression was analyzed using an ABI Prism 7900 Sequence Detection System (Applied Biosystems; Foster City, CA). Sequences for mouse primers (Integrated DNA Technologies; San Diego, CA) appear in Table 1.

Immunoblotting

Proteins were separated on 7.5% (OSMR, gp130) or 10% (Akt, ERK, phosphoSTAT3/5) polyacrylamide gels containing sodium dodecyl sulfate and transferred to nitrocellulose membranes as previously described (10). After transfer, membranes were blocked and incubated with goat anti-OSMR (R&D Systems; Minneapolis, MN; catalog #AF662), rabbit anti-STAT5A (Santa Cruz Biotechnology; Dallas, TX; catalog #sc-1081), or mouse anti-phosphoSTAT5 (Millipore Sigma; Burlington MA; catalog #05-495) primary antibodies (1:1000 dilution) overnight at 4°C. Results were visualized with appropriate horseradish peroxidase-conjugated secondary antibodies (1:15,000 dilution) (Jackson ImmunoResearch Laboratories; West Grove, PA) and SuperSignal Chemiluminescent Substrate (ThermoFisher Scientific; Waltham, MA; catalog# 34580), using a Mini-Med film processor. All immunoblots were performed in triplicate.

Serum and tissue adipokine arrays

Adipokine protein expression levels in serum (n=3 per genotype) or eWAT (n=6–7 per genotype) were assessed using mouse Proteome Profiler Adipokine Array kits (R&D Systems; Minneapolis, MN; catalog# ARY013) according to manufacturer's instructions. Briefly, eWAT was homogenized in PBS with 10 μg/mL each aprotinin, leupeptin, and pepstatin. After homogenization, Triton X-100 was added to each sample at 1% final concentration. Samples were frozen at −80°C, thawed, and centrifuged at 10,000 × g for 5 minutes at 4°C to remove cellular debris. Sample protein concentrations were quantified using a bicinchoninic acid assay with bovine serum albumin as the standard (Sigma-Aldrich, St. Louis, MO). Serum assays were performed using 100ul of mouse serum as specified in the kit instructions. Membranes were incubated with chemiluminescence reagents and then exposed to autoradiography film for times ranging from one to five minutes. Film from the five-minute exposure was used for densitometry analyses, which were performed with Image Studio Lite software (Version 3.1; Li-Cor; Lincoln, NE). Densitometry values for each adipokine were normalized to values for the reference spot on each membrane. Resulting values were then compared between genotypes.

Isolation of eWAT SVCs for immunophenotyping

Freshly excised eWAT was weighed, pooled (2–3 mice per pooled sample; 4 pooled samples per genotype), and fractionated using previously described methods (10, 13), with minor modifications (14) as briefly described here. Tissues were minced in ice-cold digestion buffer (low glucose DMEM without phenol red; 5% heat-inactivated FBS; 1 mg/ml Type II collagenase), transferred to 50 ml conical tubes, and placed into a shaking water bath at 37°C. Tissues were digested for 45 minutes at 100 rpm, with tubes being shaken vigorously by hand every 10 minutes. In the last 5 minutes of the digestion procedure, EDTA was added at a final concentration of 10mM. Each slurry was then passed through a pre-wet 100 μM cell strainer into a 50-ml conical tube and the strainer rinsed with 10 ml PBS. Slurries were centrifuged at 500x*g* for 10 minutes at 4°C. After centrifugation, floating adipocytes and supernatant were removed and RBC lysis buffer was added to the remaining SVF pellet and incubated for 5 minutes. Lysis buffer was neutralized with PBS, the SVF mixture passed through a 40μm cell strainer into a 50 ml tube, the strainer rinsed twice with 5 ml PBS, and

the tubes centrifuged at 500x*g* for 10 minutes at 4°C. The resulting SVF pellet was resuspended in 3 ml of PBS and placed on ice for processing for flow cytometry analyses. Viable cells were counted on a hemacytometer using trypan blue exclusion.

Flow cytometry analysis of SVCs

SVCs ($5 \times 10^5 – 1 \times 10^6$ cells per tube) were isolated as described above and suspended in flow cytometry staining buffer (eBioscience/Thermo Fisher; Waltham, MA; catalog #00-4222) and incubated in Fc block for 10 minutes on ice. Cells were stained with appropriate antibodies for 45 minutes at 4°C in the dark. All flow cytometry antibodies are listed in Table 2. Stained SVCs were washed twice in PBS, fixed in 1% paraformaldehyde in PBS, and analyzed on FACS Aria or FACS Calibur flow cytometers using Flow Jo software (Version 10.0; TreeStar; Ashland, OR). Adipose tissue macrophages are identified as CD45+, CD64+ (14, 15). Adipose tissue T cells are identified as CD45+, CD3+ (15). Adipose tissue B cells are identified as CD45+, CD19+, and B220+. Preadipocytes were identified as CD45-, CD31-, Sca1+ (16) and endothelial cells were identified as CD45-, CD31+. Samples were analyzed on FACS Aria or FACS Calibur flow cytometers. Data were analyzed using FlowJo software (Version 10.0; TreeStar; Ashland, OR). Gating strategies for flow cytometry analyses are based on those previously described for adipose SVCs (3, 14, 15); auto fluorescence (no antibody) controls, single stain controls, and fluorescence minus one isotype controls were used in each immunophenotyping panel for compensation settings and to determine gating. Data were normalized per gram of eWAT or as a percentage of SVCs, as indicated.

Statistical analyses

GraphPad Prism software was used for all statistical analyses (Version 7.0; GraphPad Software; La Jolla, CA), and results are expressed as mean ± SEM. Differences between genotypes were analyzed using the Student’s t-test, with results considered significant when $p<0.05$.

RESULTS

In this study, we examined the phenotypic effects of adipocyte-specific oncostatin M receptor loss ($OSMR^{FKO}$) in chow-fed male mice and littermate control $OSMR^{fl/fl}$ mice. Specifically, we examined tissue weight, insulin responsiveness, adipokine production, and stromal cell immunophenotypes in epididymal fat pads (eWAT), as well as serum adipokine production.

Adipose and non-adipose expression of oncostatin receptor subunits

We observed significant decreases in OSMR gene and protein expression in two white fat depots from $OSMR^{FKO}$ mice when compared to $OSMR^{fl/fl}$ mice (Figures 1A and 1B). The levels of gp130 gene and protein expression did not differ significantly between the control and knockout mice. There were no significant differences in either OSMR or gp130 gene and protein expression between genotypes in brown adipose tissue (Figures 1A & 1B) or in non-adipose tissues examined (Figures 1C & 1D). Notably, expression of OSM itself was

significantly increased in the eWAT of $OSMR^{FKO}$ mice (Figure 1E); this increase in OSM expression also occurs in obese high-fat fed $OSMR^{FKO}$ mice (10).

Adipose tissue response to an acute OSM challenge

Acute OSM injection in $OSMR^{fl/fl}$ mice resulted in robust phosphorylation of STAT3 and STAT5 tyrosine residues in eWAT. The reduced STAT phosphorylation in $OSMR^{FKO}$ mice (Figures 2A and 2B) indicated a substantial decrease in responsiveness to an OSM challenge. The observed effect on STAT5 phosphorylation was significant (p=0.0084; Figure 2B), while the effect on STAT3 followed the same trend but did not reach significance (p=0.074; Figure 2B). These data also suggest that adipocyte OSMR is responsible for the majority of OSM signaling in eWAT. Notably, basal levels of STAT3 and STAT5 tyrosine phosphorylation in vehicle-injected mice were lower in the $OSMR^{FKO}$ group (Figures 2A and 2B). OSM is known to induce ERKs 1&2 phosphorylation, but we did not observe a significant reduction in ERK activation following acute OSM injection in $OSMR^{FKO}$ mice compared to floxed littermate controls.

Body weight and blood glucose

Body weights did not significantly differ between $OSMR^{fl/fl}$ and $OSMR^{FKO}$ mice in any of the experimental cohorts at the time of sacrifice (Figure 3A). Fasting blood glucose levels also were not different between the two genotypes at the time of sacrifice (Figure 3B).

Insulin sensitivity and adipokine levels

As a measure of insulin sensitivity, we examined insulin-stimulated Akt phosphorylation in eWAT. Seven mice from each genotype were given intraperitoneal vehicle or insulin injections and sacrificed 10 minutes later. Most of the insulin-injected OSM^{FKO} mice had reduced Akt phosphorylation compared to floxed controls. However, when the results from all the mice were quantitated, the effects did not reach statistical significance (Figure 3C). There were no differences in total Akt levels (Figure 3C and 3D). Further, we did observe any significant changes in eWAT *Glut1* or *Glut4* gene expression levels [*Glut1* relative expression: 1.082 ± 0.125 AU ($OSMR^{fl/fl}$) vs 1.028 ±0.061 AU ($OSMR^{FKO}$); *Glut4* relative expression: 1.222 ± 0.237 AU ($OSMR^{fl/fl}$) vs 1.238 ± 0.139 AU ($OSMR^{FKO}$)] in eWAT.

Significant increases in CRP, ICAM-1, IGFBP6, and LCN2 were observed in $OSMR^{FKO}$ eWAT (Figure 4A), while ICAM-1 and FETA were elevated in $OSMR^{FKO}$ serum (Figure 4B). The elevated ICAM-1 in both serum and eWAT in $OSMR^{FKO}$ mice suggests that the eWAT may be the source of increasing circulating ICAM-1, although additional studies are required to confirm this hypothesis.

Adipokine expression in 3T3-L1 adipocytes

The lack of adipocyte OSMR signaling is associated with increased OSM expression in eWAT of $OSMR^{FKO}$ mice, both in the current study (Figure 1E) and with high-fat diet feeding (10). As shown in Figure 4A, $OSMR^{FKO}$ increased LCN2 levels in eWAT. To determine if OSM could induce *Lcn2* gene expression in a cell-autonomous manner, we studied the effects of OSM in cultured adipocytes. We observed that a 6-hour treatment with OSM strongly induced *Lcn2* expression in 3T3-L1 adipocytes. Use of the MEK inhibitor,

U0126, demonstrated that this effect was primarily ERK-dependent (Figure 5A). The efficacy of ERK inhibition was confirmed by western blotting that demonstrated a significant reduction in ERK phosphorylation following inhibitor treatment (data not shown). OSM, however, did not induce *Igfbp6* expression in adipocytes (Figure 5B). Interestingly, OSM induced *Icam1* expression and ERK inhibition further increased this effect (Figure 5C). Previous studies have reported *Crp* and *FetA* expression and secretion by adipocytes (17, 18); however, we were not able to detect either gene in our experiments in 3T3-L1 adipocytes.

Immunophenotyping of SVC populations

Though eWAT weights did not differ (Figure 6A), $OSMR^{fl/fl}$ mice had a significantly higher number of SVCs per gram of eWAT than $OSMR^{FKO}$ mice (Figure 6B). However, immunophenotyping analyses indicated significantly higher CD45+ leukocytes in $OSMR^{FKO}$ eWAT when compared to $OSMR^{fl/fl}$ eWAT (Figure 6B). While not significant, there were trends towards increased CD19+/B220+ B cells ($p=0.07$) and increased CD3+ T cells in $OSMR^{FKO}$ eWAT when compared to $OSMR^{fl/fl}$ control mice (Figures 6C and 6D, respectively). No obvious trends were observed in CD64+ adipose tissue macrophages or in endothelial cells between groups (Figures 6E and 6F). Although not statistically significant, a modest increase in Sca1+ preadipocytes was observed in the $OSMR^{FKO}$ mice (Figure 6G).

DISCUSSION

Our previous work indicates that $OSMR^{FKO}$ mice exhibit systemic insulin resistance and adipose tissue inflammation when challenged with a high-fat diet (10). Here, we studied the phenotype of $OSMR^{FKO}$ mice in the absence of a high-fat diet challenge and more closely examined the adipose tissue inflammatory profile in the $OSMR^{FKO}$ mouse. There are several significant observations from this study. Notably, adipocyte-specific OSMR deletion does not alter body mass or fasting blood glucose, but does modestly blunt adipose tissue insulin sensitivity in chow-fed mice. In addition, adipose tissue and serum pro-inflammatory adipokine expression levels are increased in chow-fed $OSMR^{FKO}$ mice. These results are consistent with the significant increase in the number of adipose tissue leukocytes (Figure 6B) and the trend towards increased T cell and B cell numbers, despite no changes in adipose tissue weight. The observed phenotypic effects in chow-fed $OSMR^{FKO}$ mice are not due to alterations in gp130 expression in adipose tissue or in gp130 and/or OSMR expression in non-adipose tissues. Taken together, these results and our previous data (10) demonstrate that the adipose tissue dysfunction in $OSMR^{FKO}$ mouse is characteristic of the genotype itself and occurs in the absence of obesity.

Our current results in $OSMR^{FKO}$ mice contrast with those of the global OSMR knockout mice fed a chow diet (19). Global OSMR knockout mice of similar age to the $OSMR^{FKO}$ mice in our study have increases in body mass, eWAT and iWAT mass, liver mass, and food intake when compared to $OSMR^{fl/fl}$ mice (19). We did not observe changes in any of these parameters in chow-fed $OSMR^{FKO}$ mice. Further, global OSMR knockout mice also exhibit significant increases in blood glucose and serum insulin and are generally glucose intolerant and insulin resistant (19), while our $OSMR^{FKO}$ mice are not. However, much like the

OSMR^{FKO} mice, global OSMR knockout mice exhibit increased adipose tissue inflammation. The vast differences in these phenotypes underscore the importance of OSMR in hematopoiesis, liver development, and other developmental functions, and suggest that many of the metabolic effects observed in the global OSMR knockout mice are due to non-adipocyte effects (19, 20, 21). Some of the molecular mechanisms by which specific disruption of adipocyte OSM-OSMR signaling axis promotes adipose tissue dysfunction still remain unclear, although our current data provide new information.

As a first step toward examining drivers of the adipose tissue dysfunction in chow-fed OSMR^{FKO} mice, we generated adipokine profiles using antibody arrays. We analyzed 38 adipokines, and found four of them were differentially expressed at significant levels: C-reactive protein (CRP), intercellular adhesion molecule 1 (ICAM-1), insulin-like growth factor binding protein 6 (IGFBP6), and lipocalin 2 (LCN2). Various cell types produce these proteins, all of which have established effects in inflammation. Immune cells can produce all four of these proteins; however, adipocytes are reported to produce at least two of them (CRP and LCN2). CRP is an acute phase protein synthesized primarily by the liver in response to cytokines or other inflammatory stimuli. Previous reports suggest that adipocytes can produce CRP in response to inflammatory stimuli (17, 18), although we were unable to detect *Crp* gene expression in our *in vitro* 3T3-L1 adipocyte experiments. Adipocytes produce LCN2 in response to pro-inflammatory cytokine exposure (22, 23, 24) and several immune cell types also produce LCN2 (25). However, substantial evidence indicates that circulating LCN2 is liver–derived and produced in response to infection or injury (26, 27), so it is not surprising that the changes we observed in LCN2 levels in this study were only at the level of the eWAT itself and not in serum (Figure 4B). The role of LCN2 in adipose tissue is generally thought to be pro-inflammatory, since increasing its expression promotes neutrophil recruitment and induces pro-inflammatory cytokine production (28, 29), although anti-inflammatory effects have been reported in other tissues (30, 31). Our *in vitro* studies clearly indicate that OSM potently induces adipocyte LCN2 expression and that this induction is ERK-dependent (Figure 5A). TNFα and IFNγ are also potent inducers of LCN2 in cultured murine adipocytes (23).

ICAM-1 is a cell surface glycoprotein found on endothelial cells and leukocytes that is induced by pro-inflammatory cytokine production and interacts with β-integrins to facilitate leukocyte migration (32). Several studies report that adipocytes can express ICAM-1 (33, 34, 35). Our *in vitro* experiments indicated that, while *Icam1* gene expression was very low in basal conditions, but OSM treatment substantially induced *Icam1* mRNA levels in adipocytes (Figure 5). The significant elevations of ICAM-1 in both serum and eWAT in OSMR^{FKO} mice when compared to floxed controls (Figure 4) is consistent with the elevated OSM levels we observe in in OSMR^{FKO} mice. Our flow cytometry data also demonstrated increased leukocyte numbers in OSMR^{FKO} adipose tissue. Given its known functions in leukocyte migration and recruitment, we hypothesize that ICAM-1 is either induced in adipocytes by immune cell-derived factors, produced by immune cells alone, or both, and may act to effectively trap leukocytes in the eWAT of the OSMR^{FKO} mouse. Further studies are required to evaluate this hypothesis.

Increased levels of fetuin A (FETA), a negative acute phase protein primarily secreted from liver (36), are associated with metabolic syndrome and insulin resistance in humans and animals (37, 38, 39). In adipose tissue, FETA serves as an endogenous toll-like receptor 4 (TLR4) ligand, where it binds fatty acids for presentation to TLR4 and subsequently triggers pro-inflammatory cytokine production via the NF-kB pathway (38). FETA can also promote macrophage migration into adipose tissue (37) and directly interfere with insulin receptor action to mediate insulin resistance (39). Data from these previous studies coincide with results obtained in $OSMR^{FKO}$ mice where we observed significant increases in serum FETA (Figure 4B) and a modest blunting of eWAT insulin signaling in comparison to $OSMR^{fl/fl}$ mice.

A family of six IGFBPs controls the activity of insulin-like growth factors; the IGFBPs all serve to inhibit IGF actions. Of these IGFBPs, IGFBP6 has garnered interest for its high specificity for IGF-II and for its IGF-independent roles, such as the promotion of apoptosis and inhibition of angiogenesis (40, 41). Literature addressing the possible role of IGFBP6 in adipose tissue is scant; however, recent evidence suggests that in some inflammatory conditions IGFBP6 may be a possible chemotactic factor (40). In this study, we observed significant increases in IGFBP6 levels in $OSMR^{FKO}$ eWAT when compared to $OSMR^{fl/fl}$ eWAT. It is possible that, if IGFBP6 acts with chemotactic ability in adipose tissue, the increased IGFBP6 in $OSMR^{FKO}$ eWAT could be partially responsible for the significantly higher number of leukocytes measured in the tissue.

Collectively, our prominent adipokine array results suggest a local pro-inflammatory environment in the adipose tissue of the $OSMR^{FKO}$ mouse that occurs in the absence of obesity. In further support of these observations, flow cytometry analyses revealed elevations of leukocytes, B cells, and T cells in $OSMR^{FKO}$ eWAT (Figure 6). While it remains unclear as to which cells in the adipose tissue are responsible for the increased adipokine production, it is clear that the loss of adipocyte OSM-OSMR signaling disrupts adipose tissue homeostasis in the absence of obesity. Likely, more than one cell type is contributing to this effect, as there is known crosstalk among cell types in adipose tissue. Future studies will more closely examine each cell type in the adipose tissue of the $OSMR^{FKO}$ mouse to better determine their roles in contributing to disrupted adipose tissue homeostasis. Despite the evident adipose tissue dysfunction in chow-fed $OSMR^{FKO}$ mice, a systemic metabolic challenge, such as an obesogenic diet, is required to produce whole-body insulin resistance while perpetuating adipose tissue inflammation in these animals (10). Taken together, these results and our previous results strongly suggest the need for intact adipocyte OSM-OSMR signaling in maintaining adipose tissue homeostasis.

Acknowledgments

Funding:

CME is supported by K01 DK106307 and JMS is supported by R01 DK052968 from the National Institutes of Health. This work used core facilities that are supported in part by COBRE (NIH P30 GM118430) and NORC (NIH P30 DK072476) center grants from the National Institutes of Health.

LITERATURE CITED

1. Greenberg AS, Obin MS. Obesity and the role of adipose tissue in inflammation and metabolism. The American Journal of Clinical Nutrition. 2006; 83:461S–465S. [PubMed: 16470013]
2. Weisberg SP, McCann D, Desai M, Rosenbaum M, Leibel RL, Ferrante AW Jr. Obesity is associated with macrophage accumulation in adipose tissue. The Journal of Clinical Investigation. 2003; 112:1796–1808. [PubMed: 14679176]
3. Cho KW, Zamarron BF, Muir LA, Singer K, Porsche CE, DelProposto JB, et al. Adipose Tissue Dendritic Cells Are Independent Contributors to Obesity-Induced Inflammation and Insulin Resistance. The Journal of Immunology. 2016; 197:3650–3661. [PubMed: 27683748]
4. Lumeng CN, Saltiel AR. Inflammatory links between obesity and metabolic disease. The Journal of Clinical Investigation. 2011; 121:2111–2117. [PubMed: 21633179]
5. Fasnacht N, Müller W. Conditional gp130 deficient mouse mutants. Seminars in Cell & Developmental Biology. 2008; 19:379–384. [PubMed: 18687405]
6. Heinrich PC, Behrmann I, Haan S, Hermanns HM, Muller-Newen G, Schaper F. Principles of interleukin (IL)-6-type cytokine signalling and its regulation. Biochemical Journal. 2003; 374:1–20. [PubMed: 12773095]
7. Zarling JM, Shoyab M, Marquardt H, Hanson MB, Lioubin MN, Todaro GJ. Oncostatin M: a growth regulator produced by differentiated histiocytic lymphoma cells. Proceedings of the National Academy of Sciences. 1986; 83:9739–9743.
8. Wallace PM, MacMaster JF, Rouleau KA, Brown TJ, Loy JK, Donaldson KL, et al. Regulation of Inflammatory Responses by Oncostatin M. The Journal of Immunology. 1999; 162:5547–5555. [PubMed: 10228036]
9. Mosley B, De Imus C, Friend D, Boiani N, Thoma B, Park LS, et al. Dual Oncostatin M (OSM) Receptors: cloning and characterization of an alternative signaling subunit conferring OSM-specific receptor activation. Journal of Biological Chemistry. 1996; 271:32635–32643. [PubMed: 8999038]
10. Elks CM, Zhao P, Grant RW, Hang H, Bailey JL, Burk DH, et al. Loss of Oncostatin M Signaling in Adipocytes Induces Insulin Resistance and Adipose Tissue Inflammation in Vivo. Journal of Biological Chemistry. 2016; 291:17066–17076. [PubMed: 27325693]
11. White UA, Stewart WC, Stephens JM. Gp130 Cytokines Exert Differential Patterns of Crosstalk in Adipocytes Both In Vitro and In Vivo. Obesity. 2011; 19:903–910. [PubMed: 21164505]
12. Sanchez-Infantes D, White UA, Elks CM, Morrison RF, Gimble JM, Considine RV, et al. Oncostatin M Is Produced in Adipose Tissue and Is Regulated in Conditions of Obesity and Type 2 Diabetes. The Journal of Clinical Endocrinology & Metabolism. 2014; 99:E217–E225. [PubMed: 24297795]
13. Grant R, Youm Y-H, Ravussin A, Dixit VD. Quantification of Adipose Tissue Leukocytosis in Obesity. Methods in Molecular Biology. 2013; 1040:195–209. [PubMed: 23852606]
14. Cho KW, Morris DL, Lumeng CN. Flow Cytometry Analyses of Adipose Tissue Macrophages. Methods in Enzymology. 2014; 537:297–314. [PubMed: 24480353]
15. Morris DL, Cho KW, DelProposto JL, Oatmen KE, Geletka LM, Martinez-Santibanez G, et al. Adipose Tissue Macrophages Function As Antigen-Presenting Cells and Regulate Adipose Tissue CD4+ T Cells in Mice. Diabetes. 2013; 62:2762–2772. [PubMed: 23493569]
16. Church C, Berry R, Rodeheffer MS. Isolation and Study of Adipocyte Precursors. Methods in Enzymology. 2014; 537:31–46. [PubMed: 24480340]
17. Calabro P, Chang DW, Willerson JT, Yeh ETH. Release of C-Reactive Protein in Response to Inflammatory Cytokines by Human Adipocytes: Linking Obesity to Vascular Inflammation. Journal of the American College of Cardiology. 2005; 46:1112–1113. [PubMed: 16168299]
18. Memoli B, Procino A, Calabrò P, Esposito P, Grandaliano G, Pertosa G, et al. Inflammation may modulate IL-6 and C-reactive protein gene expression in the adipose tissue: the role of IL-6 cell membrane receptor. American Journal of Physiology-Endocrinology and Metabolism. 2007; 293:E1030–E1035. [PubMed: 17652155]
19. Komori T, Tanaka M, Senba E, Miyajima A, Morikawa Y. Lack of Oncostatin M Receptor β Leads to Adipose Tissue Inflammation and Insulin Resistance by Switching Macrophage Phenotype. Journal of Biological Chemistry. 2013; 288:21861–21875. [PubMed: 23760275]

20. Tamura S, Morikawa Y, Tanaka M, Miyajima A, Senba E. Developmental expression pattern of oncostatin M receptor β in mice. Mechanisms of Development. 2002; 115:127–131. [PubMed: 12049776]
21. Tanaka M, Hirabayashi Y, Sekiguchi T, Inoue T, Katsuki M, Miyajima A. Targeted disruption of oncostatin M receptor results in altered hematopoiesis. Blood. 2003; 102:3154–3162. [PubMed: 12855584]
22. Yan Q-W, Yang Q, Mody N, Graham TE, Hsu C-H, Xu Z, et al. The Adipokine Lipocalin 2 Is Regulated by Obesity and Promotes Insulin Resistance. Diabetes. 2007; 56:2533–2540. [PubMed: 17639021]
23. Zhao P, Elks CM, Stephens JM. The induction of lipocalin-2 expression in vivo and in vitro. Journal of Biological Chemistry. 2014; 289:5960–5969. [PubMed: 24391115]
24. Zhao P, Stephens JM. STAT1, NF-κB and ERKs play a role in the induction of lipocalin-2 expression in adipocytes. Molecular Metabolism. 2013; 2:161–170. [PubMed: 24049731]
25. Flo TH, Smith KD, Sato S, Rodriguez DJ, Holmes MA, Strong RK, et al. Lipocalin 2 mediates an innate immune response to bacterial infection by sequestrating iron. Nature. 2004; 432:917. [PubMed: 15531878]
26. Meier EM, Pohl R, Rein-Fischboeck L, Schacherer D, Eisinger K, Wiest R, et al. Circulating lipocalin 2 is neither related to liver steatosis in patients with non-alcoholic fatty liver disease nor to residual liver function in cirrhosis. Cytokine. 2016; 85:45–50. [PubMed: 27288631]
27. Sultan S, Pascucci M, Ahmad S, Malik I, Bianchi A, Ramadori P, et al. Lipocalin-2 is a major acute-phase protein in a rat and mouse model of sterile abscess. Shock. 2012; 37:191–196. [PubMed: 22249220]
28. Catalán V, Gómez-Ambrosi J, Rodríguez A, Ramírez B, Silva C, Rotellar F, et al. Increased adipose tissue expression of lipocalin-2 in obesity is related to inflammation and matrix metalloproteinase-2 and metalloproteinase-9 activities in humans. Journal of Molecular Medicine. 2009; 87:803. [PubMed: 19466389]
29. Law IKM, Xu A, Lam KSL, Berger T, Mak TW, Vanhoutte PM, et al. Lipocalin-2 Deficiency Attenuates Insulin Resistance Associated With Aging and Obesity. Diabetes. 2010; 59:872–882. [PubMed: 20068130]
30. Moschen AR, Adolph TE, Gerner RR, Wieser V, Tilg H. Lipocalin-2: A Master Mediator of Intestinal and Metabolic Inflammation. Trends in Endocrinology & Metabolism. 2017; 28:388–397. [PubMed: 28214071]
31. Toyonaga T, Matsuura M, Mori K, Honzawa Y, Minami N, Yamada S, et al. Lipocalin 2 prevents intestinal inflammation by enhancing phagocytic bacterial clearance in macrophages. Scientific Reports. 2016; 6:35014. [PubMed: 27734904]
32. Aljada A, Saadeh R, Assian E, Ghanim H, Dandona P. Insulin Inhibits the Expression of Intercellular Adhesion Molecule-1 by Human Aortic Endothelial Cells through Stimulation of Nitric Oxide1. The Journal of Clinical Endocrinology & Metabolism. 2000; 85:2572–2575. [PubMed: 10902810]
33. Elgazar-Carmon V, Rudich A, Hadad N, Levy R. Neutrophils transiently infiltrate intra-abdominal fat early in the course of high-fat feeding. J Lipid Res. 2008; 49:1894–1903. [PubMed: 18503031]
34. Permana PA, Menge C, Reaven PD. Macrophage-secreted factors induce adipocyte inflammation and insulin resistance. Biochemical and Biophysical Research Communications. 2006; 341:507–514. [PubMed: 16427608]
35. Soukas A, Socci ND, Saatkamp BD, Novelli S, Friedman JM. Distinct Transcriptional Profiles of Adipogenesis in Vivo and in Vitro. Journal of Biological Chemistry. 2001; 276:34167–34174. [PubMed: 11445576]
36. Triffitt JT, Gebauer U, Ashton BA, Owen ME, Reynolds JJ. Origin of plasma α2HS-glycoprotein and its accumulation in bone. Nature. 1976; 262:226. [PubMed: 934340]
37. Chatterjee P, Seal S, Mukherjee S, Kundu R, Mukherjee S, Ray S, et al. Adipocyte Fetuin-A Contributes to Macrophage Migration into Adipose Tissue and Polarization of Macrophages. Journal of Biological Chemistry. 2013; 288:28324–28330. [PubMed: 23943623]

38. Pal D, Dasgupta S, Kundu R, Maitra S, Das G, Mukhopadhyay S, et al. Fetuin-A acts as an endogenous ligand of TLR4 to promote lipid-induced insulin resistance. Nature Medicine. 2012; 18:1279.

39. Srinivas PR, Wagner AS, Reddy LV, Deutsch DD, Leon MA, Goustin AS, et al. Serum alpha 2-HS-glycoprotein is an inhibitor of the human insulin receptor at the tyrosine kinase level. Molecular Endocrinology. 1993; 7:1445–1455. [PubMed: 7906861]

40. Alunno A, Bistoni O, Manetti M, Cafaro G, Valentini V, Bartoloni E, et al. Insulin-Like Growth Factor Binding Protein 6 in Rheumatoid Arthritis: A Possible Novel Chemotactic Factor? Frontiers in Immunology. 2017; 8:554. [PubMed: 28572803]

41. Bach LA. Recent insights into the actions of IGFBP-6. Journal of Cell Communication and Signaling. 2015; 9:189–200. [PubMed: 25808083]

What is already known about this subject?

- Adipose tissue oncostatin M (OSM) protein and gene expression are significantly induced in obese rodents and in people with obesity.
- Obese mice with adipocyte-specific deletion of the oncostatin M receptor (OSMR) exhibit systemic insulin resistance and increased adipose tissue immune cell infiltration.

What does our study add?

- Altered pro-inflammatory adipokine production observed in the adipocyte-specific OSMR knockout mouse occurs in the absence of high-fat diet-induced obesity.
- Adipose tissue immune cell infiltration and adipose tissue dysfunction are present in non-obese adipocyte-specific OSMR knockout mice.

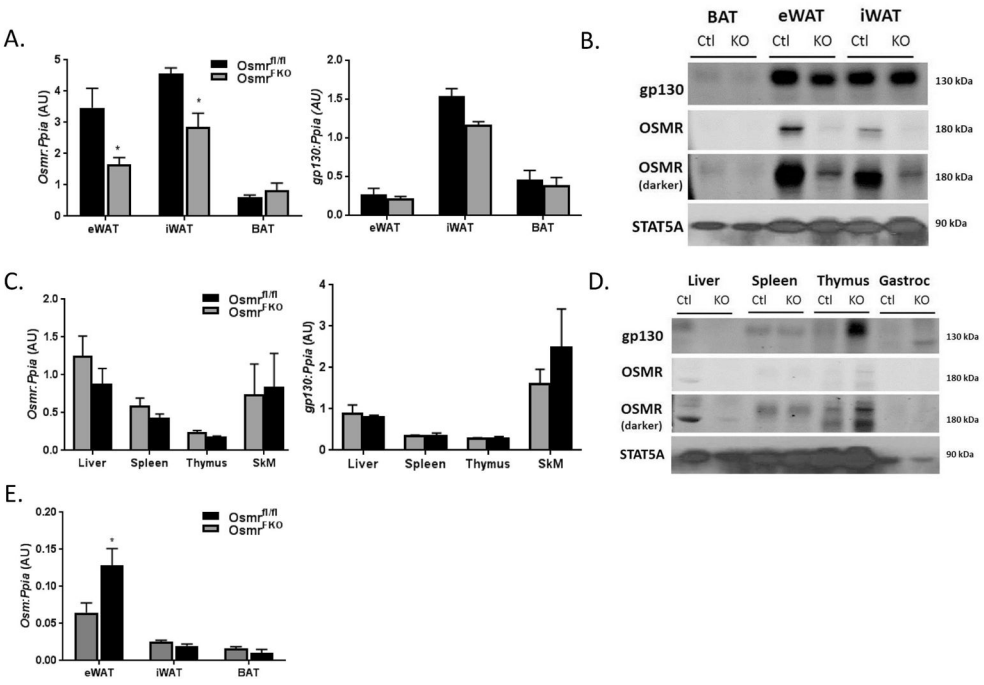

Figure 1. Expression levels of OSMR and gp130 are not altered in non-adipose tissues

Tissue expression of OSMR and gp130 in various adipose depots at the A) gene and B) protein levels in $OSMR^{fl/fl}$ (CTL) and $OSMR^{FKO}$ (KO) chow-fed mice. Non-adipose tissue expression of OSMR and gp130 at the C) gene and D) protein levels was also measured. E) Gene expression of OSM itself was also measured in various adipose depots. Total RNA in various tissues was purified and analyzed by real-time PCR. Cyclophilin A (*Ppia*) was used as an endogenous control. Protein (100 ug for adipose tissues, 50 ug for all other tissues) was subjected to Western blot analysis. Data are shown as mean ± SEM. For PCR, n=8 per genotype (eWAT), n=3–4 per genotype (inguinal WAT (iWAT), brown adipose tissue (BAT), other tissues). ***$p < 0.001$, *$p<0.05$ vs. $OSMR^{fl/fl}$. AU, arbitrary units.

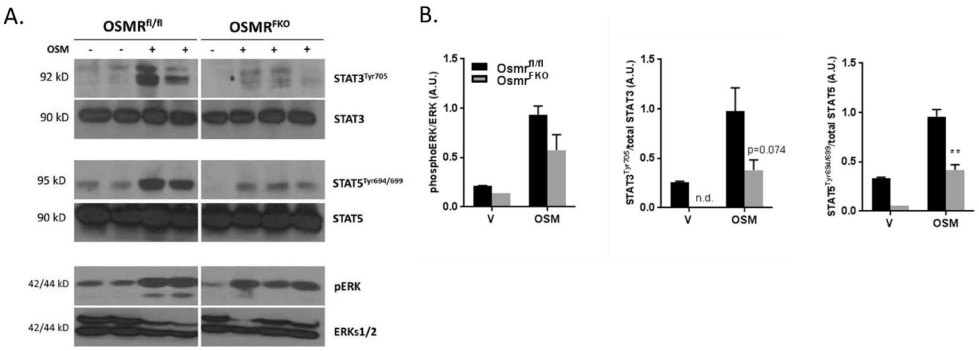

Figure 2. OSMR^{FKO} mice are less responsive to an acute OSM challenge

A) Effects of acute OSM or vehicle injection (15 min) on STAT and ERK phosphorylation in eWAT of chow-fed OSMR$^{fl/fl}$ (n=4) or OSMR^{FKO} mice (n=4). 75 ug protein was subjected to Western blot analysis. B) Densitometry analyses were conducted using Image Studio software. Data are shown as mean ± SEM and are representative of two independent experiments. AU, arbitrary units.

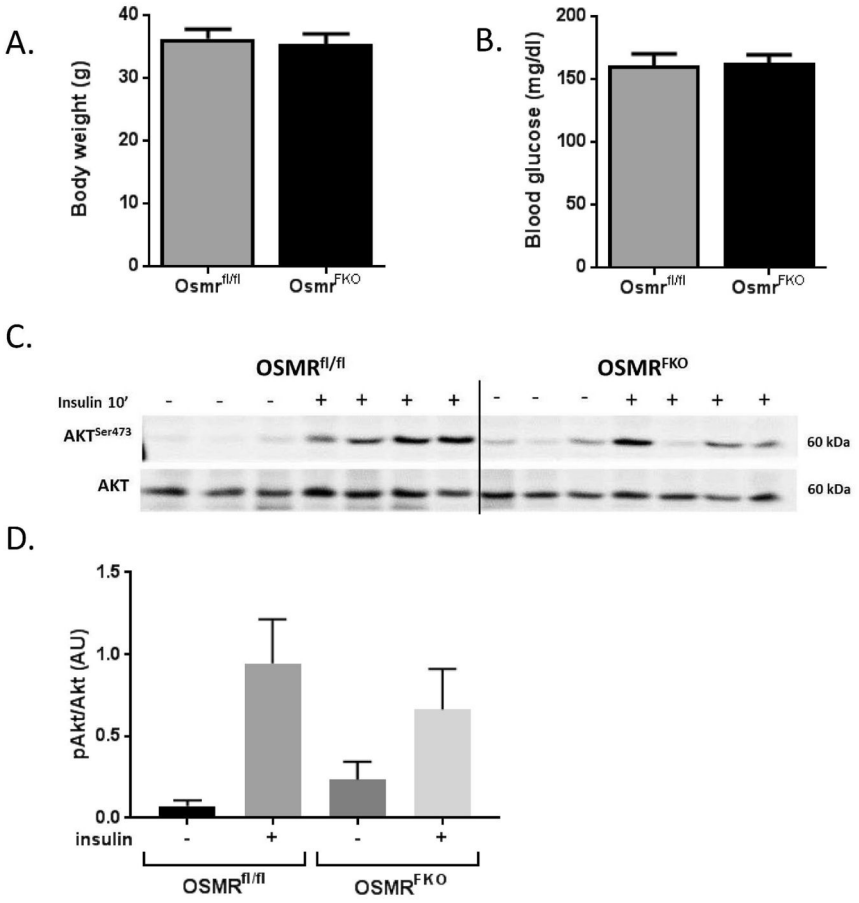

Figure 3. OSMR^{FKO} mice exhibit a modest blunting of insulin-induced Akt phosphorylation

A) Body weights, B) 4-hour fasting blood glucose, and C) protein expression levels of Akt, phosphoAkt, and phosphoERK in eWAT from chow-fed OSMR$^{fl/fl}$ and OSMR^{FKO} (KO) mice. Body weights and blood glucose levels were not significantly different between genotypes. 100 ug protein was subjected to Western blot analysis. KO mice exhibited a slight diminution in Akt phosphorylation (S473) in eWAT. Densitometry analysis of D) pAkt/Akt ratio was conducted using Image Studio software. For vehicle injections, n=3 per genotype and for insulin injections, n=4 per genotype. Data are shown as mean ± SEM. AU, arbitrary units.

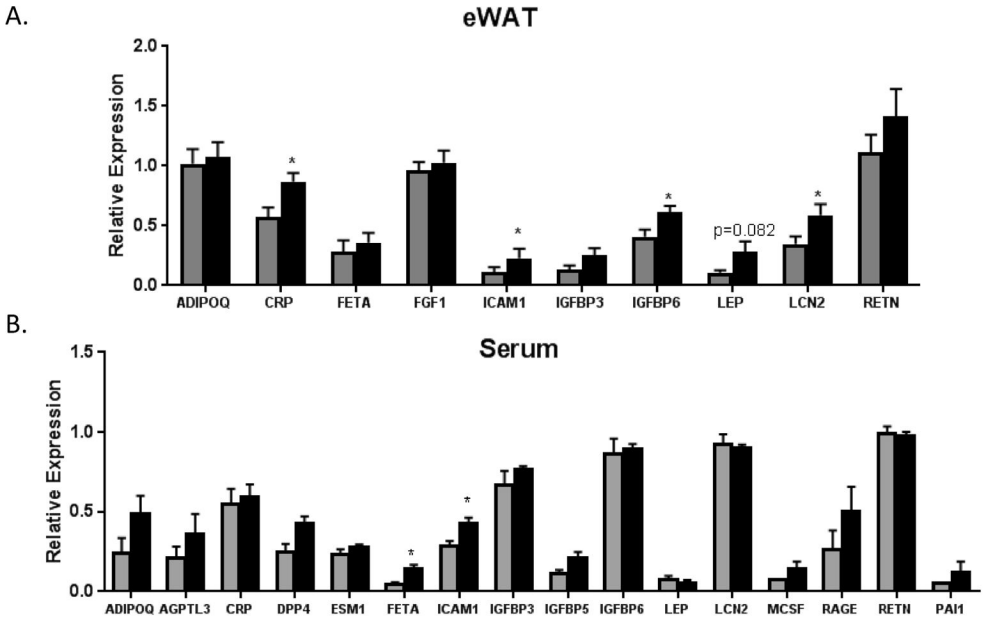

Figure 4. Increased pro-inflammatory adipokine expression in eWAT and serum of OSMR^{FKO} mice

Protein expression levels of various adipokines in A) eWAT (n=6–7 per genotype) and B) serum (n=3 per genotype) of chow-fed OSMR$^{fl/fl}$ (grey bars) and OSMR^{FKO} (black bars) mice. CRP, ICAM-1, IGFBP6, and LCN2 expression levels were significantly increased in eWAT of the OSMR^{FKO} mice when compared to OSMR$^{fl/fl}$ mice, and we observed significant increases in FETA and ICAM-1 in the serum of OSMR^{FKO} mice when compared to OSMR$^{fl/fl}$ mice. Data are presented as mean ± SEM. *$p<0.05$ vs. OSMR$^{fl/fl}$.

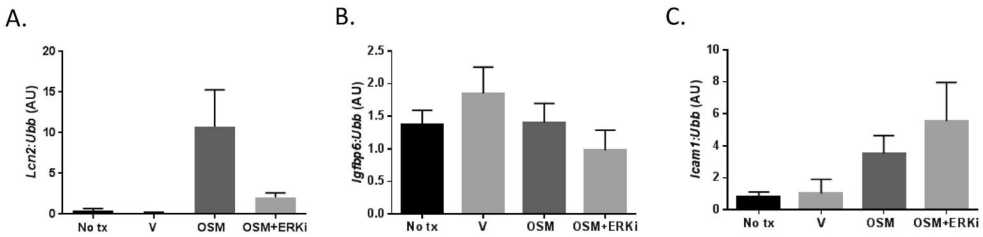

Figure 5. Adipokine gene expression in 3T3-L1 adipocytes in response to OSM treatment and/or ERK inhibition

Fully differentiated 3T3-L1 adipocytes were treated with 1 nM or OSM or vehicle for 6 hours in the presence/absence of the ERK inhibitor U0126. Gene expression levels of A) *Lcn2*, B) *Igfbp6*, C) *Icam1*, *Crp*, and *FetA* were assessed, but *Crp* and *FetA* were not detected. Total RNA was purified from cells and analyzed by real-time PCR. Ubiquitin b (*Ubb*) was used as an endogenous control.

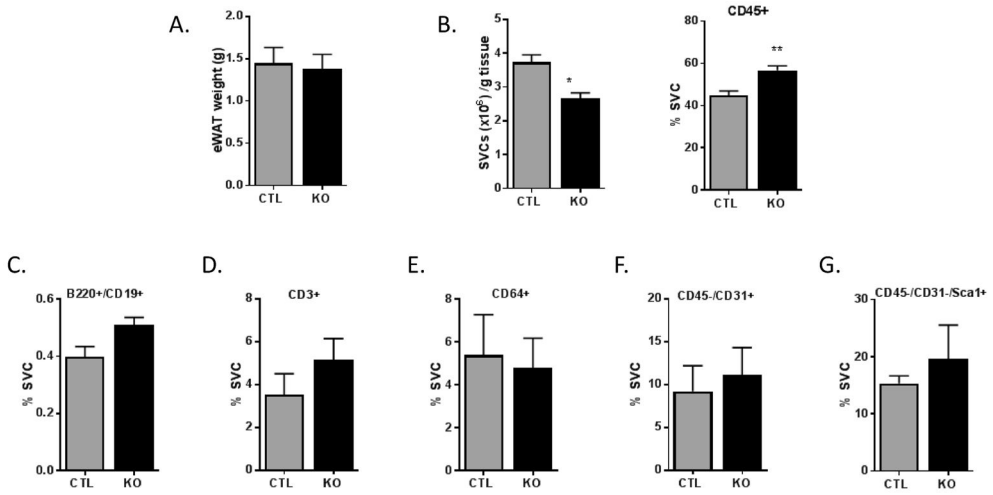

Figure 6. Leukocyte accumulation and altered immune cell populations in eWAT of OSMR^{FKO} mice

A) Epididymal fat pad (eWAT) weight, B) number of SVF cells per gram eWAT and CD45+ leukocytes as determined by flow cytometry in chow-fed OSMR$^{fl/fl}$ (CTL; grey bars) and OSMR^{FKO} (KO; black bars) mice (n=4 groups of pooled tissue per genotype; 2–3 mice per pool). Quantification of eWAT stromal vascular cells was performed using flow cytometry and data are presented as % SVCs for C) B cells (CD19+/B220+), D) T cells (CD3+), E) macrophages (CD64+), F) endothelial cells (CD31+), and G) preadipocytes (CD31-/Sca1+). Data presented are mean ± SEM. *p<0.05 and ** p<0.01 vs. OSMR$^{fl/fl}$.

Table 1

Sequences for qPCR primers used in this study.

Gene	Forward Sequence	Reverse Sequence
Crp	CAG CAG CAT CCA TAG CCA T	TGC TTC CAG AGA CAC ATA GGA
FetA (Ahsg)	CTT CAG GGA TTC AAA CAG GTC T	CAA AGC ATG GCA AGT GGT C
Glut1 (Slc2a1)	AGT TCG GCT ATA ACA CTG GTG	GTG GTG AGT GTG GTG GAT G
Glut4 (Slc2a4)	TCT TAT TGC AGC GCC TGA G	GAG AAT ACA GCT AGG ACC AGT G
gp130	AGG AGA AAT AGA AGC CAT AGT CG	TGG AAG GAT CAG GAA CAT TAG G
Icam1	CTG TGC TTT GAG AAC TGT GG	GGT CCT TGC CTA CTT GCT G
Igfbp6	TCT ATG TGC CAA ACT GTG ACC	CTG AGT GCT TCC TTG ACC ATC
Lcn2	TGC AAG TGG CCA CCA CGG AC	GCA TTG GTC GGT GGG GAC AGA GA
Osmr	CGT TCC CCT GTG AGG CCG AG	TCC TCC AAG ACT TCG CTT CGG G
Ppia	CCA CTG TCG CTT TTC GCC GC	TGC AAA CAG CTC GAA GGA GAC GC
Ubb	CCA GTG GGC AGT GAT GG	GCT TAC CAT GCA ACA AAA CCT

Table 2

Flow cytometry antibodies used in this study.

Antibody	Clone	Vendor
CD45.2	104	eBioscience/ThermoFisher
CD64	X54-5/7.1	BD Biosciences
CD31	390	eBioscience/ThermoFisher
CD19	1D3	eBioscience/ThermoFisher
B220	RA3-6B2	eBioscience/ThermoFisher
CD3	145-2C11	eBioscience/ThermoFisher
Sca1	D7	eBioscience/ThermoFisher
CD16/CCD32 (Fc block)	93	eBioscience/ThermoFisher
Mouse IgG2aκ	eBM2a	eBioscience/ThermoFisher
Mouse IgG1κ	P3.6.2.8.1	eBioscience/ThermoFisher
Rat IgG2aκ	eBR2a	eBioscience/ThermoFisher
Armenian hamster IgG	eBio299Arm	eBioscience/ThermoFisher